ISEIS

Journal of Environmental Informatics 14(1) 51-65 (2009)

Journal of Environmental Informatics

www.iseis.org/jei

3D Model for Evaluation of Pollutant Concentration Distributions from Land-Based Sources of the Caspian Sea Region — Regional Study, Southern Part of the Caspian Sea

M. Abbaspour[1] and M. H. Nobakhti[2,*]

[1]*Sharif University of Technology, Tehran 1477893855, Iran*
[2]*Islamic Azad University, Research and Science Campus, Tehran 1477893855, Iran*

Received 20 December 2005; revised 3 December 2006; accepted 7 May 2009; published online 10 September 2009

ABSTRACT. An unstructured grid, finite-volume, and three-dimensional (3D) primitive equation ocean model has been developed to predict oceanic pollutant dispersions in depth and surface of the Caspian Sea for non-chemical reactions of dissolved constituents. The model consists of momentum, continuity, temperature, salinity, and density equations. Physical and mathematical closure has been achieved using Mellor and Yamada turbulent closure sub-models. Since determining a practical definition of salinity that enjoys acceptable accuracy is difficult; therefore, various definitions have been used in this work. A recent definition of salinity stated in the UNESCO Practical Salinity Scale of 1978, PSS78, defines salinity in terms of a conductivity ratio. However, this is dimensionless and is not useful for computational methods. The old definition of salinity is "Total amount of solid materials in grams dissolved in one kilogram of sea water when all the carbonate has been converted to oxide the bromine and iodine replaced by chlorine and all organic matter completely oxidized". Although used here but it is difficult to be used routinely explanatory this definition for computational method. We assume S (Salinity) = ΣS_i and ρ_t (total density) = $\rho(\Theta,S_i) \equiv \rho(\Theta, S_1, S_2, S_3, \ldots)$ where in ΣS_i, and S_1 just is supposed salinity and other S_2, S_3, … are considered as pollutants. The irregular bottom slope is represented by a sigma coordinate transformation, and the horizontal grids comprise unstructured triangular cells. The finite-volume method (FVM) used in this model combines the advantages of a finite-element method (FEM) for geometric flexibility and a finite-difference method (FDM) for simple discrete computation. The model was applied to the southern Caspian Sea region; including a semi-enclosed coastal ocean and inputs of geographical southern Caspian Sea which include, wind forcing, heat fluxes, precipitation via evaporation, river discharge with pollutant data and temperature. The outputs of these equations were pollutant, velocity and temperature distribution in southern Caspian Sea. A software was developed for this model by the name of SPAUM (Sea Pollutant Azad University Model).

Keywords: caspian sea, finite-volume, ocean, pollutant, unstructured grid

1. Introduction

The Caspian Sea is the largest enclosed body of water on Earth, with a surface area of more than 373,000 square kilometers. It can be divided into three basins: northern, middle, and southern. In the northern part the average depth of water is less than 10 meters, whilst in the middle and southern parts, the maximum depths are 788 meters and 1025 meters respectively. The Caspian Sea has two types of cyclonic eddy currents (counter-clockwise) in central and south-eastern regions. In the southern coastal regions of the Caspian Sea the currents are generally directed towards the northwest, north, south-east and south. Baroclinic, Seiches and inertial currents also play an important role in the local circulation patterns. Due to the depth of water in the Caspian Sea, oceanic numerical methods may be used for finding its currents and distribution of temperature and pollutant.

Three numerical methods have been widely used in ocean models. A few examples are the finite difference method (Blumberg and Mellor, 1987; Haidvogel et al., 1991; Blumberg, 1994), the finite element method (Lynch and Naimie, 1993; Naimie, 1996), and the finite volume method (Chen, 2002). All of these models use different mesh types and solve concurrent momentum, continuity, temperature, salinity, density and turbulence closure sub-model equations in order to find ocean currents and distributions of temperature and salinity. However, they can not analyze oceanic pollutant dispersions. All of these models use a simple definition for salinity which is the total amount of dissolved material in grams in one kilogram of sea water. However, this is not always practical since the dissolved materials (e.g. gasses) are almost impossible to be measured in reality. Sea-water could be evaporated to attain the derived dryness, because chlorides are lost in the last stages of drying (Sverdrup et al., 1942).

To avoid these difficulties, the International Council for

* Corresponding author. Tel.: +98 21 88344087; fax: +98 21 88344086.
E-mail address: mh_nobakhti@ceers.org (M. H. Nobakhti).

ISSN: 1726-2135 print/1684-8799 online
 doi:10.3808/jei.200900153

the Exploration of the Sea set up a commission in 1889 which recommended that salinity be defined as the total amount of solid materials in grams dissolved in one kilogram of sea water when all the carbonate has been converted to oxide, the bromine and iodine replaced by chlorine and all organic matter completely oxidized. The definition was published in 1902.

The Caspian Sea is under the constant threat of pollution. There are various sources of pollution, which can be classified as follows: 1) river flow; 2) onshore industrial and municipal waste water; 3) offshore and onshore oil extraction; 4) sea level fluctuations, resulting in flooding of coastal zones, where many oil wells are still operating. Intensive oil and gas exploration and extraction in the Caspian Sea region have resulted in extensive air, water and land pollution, wildlife and plant degradation, exhaustion of natural resources, ecosystem disturbance, desertification and considerable losses in biological and landscape diversity. The cost of incurred environmental damages often exceeds the revenues gained from exploitation of natural resources. Negative environmental changes cause growth of human morbidity and mortality. Life expectancy in the Caspian littoral states is lower by 15 ~ 20 years than in developed countries.

The present work was carried out to estimate the contamination in the south part of Caspian Sea. At the end, the quantity of each contamination was calculated and reported. The introduced model calculate the effect of contamination entering from different rivers to sea, considering other parameters like rain, evaporation, temperature and Carioles force, then shows the distribution for each contamination separately in the sea. At first the mathematical model was produced. By using the sigma coordination system, the model solved numerically with finite volume method. In order to evaluate the results, the model was checked in a controlled area. After the outputs were proved to be correct; the model was used for Caspian Sea to generate the required results.

2. Governing Equations

The model uses orthogonal curvilinear coordinates in the horizontal and the sigma coordinate system in the vertical direction (Mellor et al., 2002).

Let x_1 and x_2 be the horizontal coordinates and z the vertical coordinate of a right handed orthogonal curvilinear coordinate system.

The equations will be written in the z system before transforming to the sigma coordinate system in the vertical direction. Let u_1 and u_2 be the velocities in the x_1 and x_2 directions and w be the velocity in the vertical direction. For increasing accuracy, equations are defined:

$$h_1\delta x_1 = \Delta x_1 \& h_2\delta x_2 = \Delta x_2 \tag{1}$$

where h_1 and h_2 are the metric coefficients and ds is the length of a segment in (x_1, x_2, z) space satisfying the identity:

$$ds^2 = h_1^2 dx_1^2 + h_2^2 dx_2^2 + dz^2 \tag{2}$$

The governing equations are simplified by assuming that the fluid is incompressible. Consequently variations in density are ignored except when the density is multiplied by gravitational acceleration; thus retaining the important stratification (i.e. buoyancy) effects. This is the so-called Boussinesq approximation.

The governing equations consist of the following continuity, momentum, temperature, salinity, and density equations:

$$\frac{\partial u_1}{\partial t} + \frac{1}{h_1 h_2}\left[\frac{\partial}{\partial x_1}\left(h_2 u_1^2\right) + \frac{\partial}{\partial x_2}\left(h_1 u_1 u_2\right)\right] + \frac{\partial}{\partial z}\left(w u_1\right) + \frac{u_1 u_2}{h_1 h_2}\frac{\partial h_1}{\partial x_2} - \frac{u_2^2}{h_1 h_2}\frac{\partial h_2}{\partial x_1} - f u_2 = -\frac{1}{\rho_0 h_1}\frac{\partial P}{\partial x_1} + \frac{1}{h_1 h_2}\left[\frac{\partial}{\partial x_1}\left(h_2\tau_{12}\right) + \frac{\partial}{\partial x_2}\left(h_1\tau_{22}\right) + \tau_{12}\frac{\partial h_2}{\partial x_2} - \tau_{11}\frac{\partial h_1}{\partial x_2}\right] + \frac{\partial}{\partial z}\left(K_M\frac{\partial u_1}{\partial z}\right) \tag{3}$$

$$\frac{\partial u_2}{\partial t} + \frac{1}{h_1 h_2}\left[\frac{\partial}{\partial x_1}\left(h_2 u_1 u_2\right) + \frac{\partial}{\partial x_2}\left(h_2 u_2^2\right)\right] + \frac{\partial}{\partial z}\left(w u_2\right) + \frac{u_1 u_2}{h_1 h_2}\frac{\partial h_2}{\partial x_1} - \frac{u_1^2}{h_1 h_2}\frac{\partial h_1}{\partial x_2} - f u_1 = -\frac{1}{\rho_0 h_2}\frac{\partial P}{\partial x_2} + \frac{1}{h_1 h_2}\left[\frac{\partial}{\partial x_1}\left(h_2\tau_{12}\right) + \frac{\partial}{\partial x_2}\left(h_1\tau_{22}\right) + \tau_{12}\frac{\partial h_2}{\partial x_2} - \tau_{11}\frac{\partial h_1}{\partial x_2}\right] + \frac{\partial}{\partial z}\left(K_M\frac{\partial u_2}{\partial z}\right) \tag{4}$$

$$\frac{\rho}{\rho_0}g = -\frac{1}{\rho_0}\frac{\partial P}{\partial z} \tag{5}$$

$$P = P_a + \rho_0 g\eta + g\int_z^o \rho(\xi)\,d\xi \tag{6}$$

$$\tau_{11} = 2A_M\left[\frac{1}{h_1}\frac{\partial u_1}{\partial x_1} + \frac{u_2}{h_1 h_2}\frac{\partial h_1}{\partial x_2}\right] \tag{7}$$

$$\tau_{12} = A_M\left[\frac{h_1}{h_2}\frac{\partial}{\partial x_2}\left(\frac{u_1}{h_1}\right) + \frac{h_2}{h_1}\frac{\partial}{\partial x_1}\left(\frac{u_2}{h_2}\right)\right] = \tau_{21} \tag{8}$$

$$\tau_{22} = 2A_M\left[\frac{1}{h_2}\frac{\partial u_2}{\partial x_2} + \frac{u_1}{h_1 h_2}\frac{\partial h_2}{\partial x_1}\right] \tag{9}$$

$$\frac{\partial}{\partial x_1}\left(h_2 u_1\right) + \frac{\partial}{\partial x_2}\left(h_1 u_2\right) + h_1 h_2\frac{\partial w}{\partial z} = 0 \tag{10}$$

$$\frac{\partial\Theta}{\partial t} + \frac{1}{h_1 h_2}\left[\frac{\partial}{\partial x_1}\left(h_2 u_1\Theta\right) + \frac{\partial}{\partial x_2}\left(h_1 u_2\Theta\right)\right] + \frac{\partial}{\partial z}\left(w\Theta\right) = \frac{1}{h_1 h_2}\left[\frac{\partial}{\partial x_1}\left(A_H\frac{h_2}{h_1}\frac{\partial\Theta}{\partial x_1}\right) + \frac{\partial}{\partial x_2}\left(A_H\frac{h_1}{h_2}\frac{\partial\Theta}{\partial x_2}\right)\right] + \frac{\partial}{\partial z}\left(K_H\frac{\partial\Theta}{\partial z}\right) + \frac{\partial Q_S}{\partial z} \tag{11}$$

$$\frac{\partial S_i}{\partial t}+\frac{1}{h_1h_2}\left[\frac{\partial}{\partial x_1}\left(h_2u_1S_i\right)+\frac{\partial}{\partial x_2}\left(h_1u_2S_i\right)\right]+\frac{\partial}{\partial z}\left(wS_i\right)$$
$$=\frac{1}{h_1h_2}\left[\frac{\partial}{\partial x_1}\left(A_H\frac{h_2}{h_1}\frac{\partial S_i}{\partial x_1}\right)+\frac{\partial}{\partial x_2}\left(A_H\frac{h_1}{h_2}\frac{\partial S_i}{\partial x_2}\right)\right]+\frac{\partial}{\partial z}\left(K_H\frac{\partial S_i}{\partial z}\right) \quad (12)$$

$$\rho=\rho\left(\Theta,S_i\right) \quad (13)$$

where τ_{11}, τ_{12} and τ_{22} are the components of the symmetric Reynolds stress tensor in the horizontal plane and quantity A_M is the horizontal diffusivity, while K_M denotes vertical diffusivity. Both quantities are determined by turbulent mixing in the fluid column. The variable ρ is the fluid density, ρ_0 the reference density, g the gravitational acceleration, p the pressure, and f the Coriolis parameter. Note that $f=2\Omega\sin\phi$, where Ω is the angular rotation of the Earth in radians and ϕ is the latitude. p_a is the atmospheric pressure and η is the free surface height. The form of the Coriolis terms is general in the sense that no approximations such as the *f*-plane or β-plane have been invoked. The former approximation ignores the latitudinal variations of f, while the latter makes a linear approximation $f=f_0+\beta y$ where β is $\partial f/\partial y$ and y is the coordinate in the latitudinal direction equal to $R\phi$, where R is the radius of the Earth. K_H is the vertical and A_H the horizontal eddy diffusivities due to turbulent mixing of heat and salt and other in the water column. The density variations in the ocean are of fundamental importance in determining the ocean circulation.

Density ρ is a complex function of the temperature T, salinity (pollutants) S and the pressure (or equivalently depth z). It is common to take pressure effects into account by considering ρ to be potential density, which is only a function of the potential temperature Θ and salinity (pollutants) S_i, where w is the index of pollutant. The potential temperature Θ is usually referred to the atmospheric pressure, meaning that it is the temperature attained by a fluid parcel of in-situ temperature T and salinity (pollutants) S_i brought adiabatically from depth z to the surface. The baroclinic pressure gradient terms in the momentum equations and the vertical stability of the fluid column can be evaluated accurately using the horizontal and vertical gradients of potential density ρ, which can be regarded as a function of Θ and S_i. The turbulence in the so-called level 2.25 models is characterized by two quantities, the turbulence kinetic energy $q^2/2$ and the turbulence macro-scale l. These two-equation models of turbulence are governed by the following equations:

$$\frac{\partial}{\partial t}\left(q^2\right)+\frac{1}{h_1h_2}\left[\frac{\partial}{\partial x_1}\left(h_2u_1q^2\right)\frac{\partial}{\partial x_2}\left(h_1u_2q^2\right)\right]+\frac{\partial}{\partial z}\left(wq^2\right)=2K_M\cdot$$
$$\left[\left(\frac{\partial u_1}{\partial z}\right)^2+\left(\frac{\partial u_2}{\partial z}\right)^2\right]+2K_H\frac{g}{\rho0}\frac{\partial\rho}{\partial z}-\frac{2q^3}{B_1l}+\frac{1}{h_1h_2}\left[\frac{\partial}{\partial x_1}\left(A_H\frac{h_2}{h_1}\frac{\partial q^2}{\partial x_1}\right)\right.$$
$$\left.+\frac{\partial}{\partial\chi_2}\left(A_H\frac{h_1}{h_2}\frac{\partial q^2}{\partial x_2}\right)\right]+\frac{\partial}{\partial z}\left(K_q\frac{\partial q^2}{\partial z}\right) \quad (14)$$

$$\frac{\partial}{\partial t}\left(q^2l\right)+\frac{1}{h_1h_2}\left[\frac{\partial}{\partial x_1}\left(h_2u_1q^2l\right)\frac{\partial}{\partial x_2}\left(h_1u_2q^2l\right)\right]+\frac{\partial}{\partial z}\left(wq^2\right)=K_ME_1l\cdot$$
$$\left[\left(\frac{\partial u_1}{\partial z}\right)^2+\left(\frac{\partial u_2}{\partial z}\right)^2\right]+K_HE_3l\frac{g}{\rho0}\frac{\partial\rho}{\partial z}-\frac{q^3}{B_1}\left[1+E_2\left(\frac{l}{\kappa\mathbb{L}}\right)^2\right]+\frac{1}{h_1h_2}\cdot$$
$$\left[\frac{\partial}{\partial x_1}\left(A_H\frac{h_2}{h_1}\frac{\partial}{\partial x_1}\left(q^2l\right)\right)+\frac{\partial}{\partial x_2}\left(A_H\frac{h_1}{h_2}\frac{\partial}{\partial x_2}\left(q^2l\right)\right)\right]+\frac{\partial}{\partial z}\left(K_q\frac{\partial}{\partial z}\left(q^2l\right)\right) \quad (15)$$

Vertical mixing coefficients K_M and K_H in the fully turbulent mixed layers at the surface and the bottom are obtained by second order closure model of turbulence based on the work of Mellor and Yamada (1982).

Second order closure relates the vertical mixing coefficients K_M, K_H and K_q to the turbulence scales q and l as follows:

$$K_M=lqS_M$$
$$K_H=lqS_H \quad (16)$$
$$K_q=lqS_q$$

where S_M, S_H and S_q are stability functions determined by algebraic relations derived analytically from simplifications made to the full second momentum closure model:

$$S_M=A_1\frac{\left(1-\frac{6A_1}{B_1}-3C_1\right)+9\left(2A_1+A_2\right)S_HG_H}{\left(1-9A_1A_2G_H\right)} \quad (17)$$

$$S_H=A_2\frac{1-6A_1/B_1}{1-3A_2G_H\left(6A_1+B_2\right)} \quad (18)$$

$$S_q=0.2 \quad (19)$$

$$G_H=\frac{l^2}{q^2}\frac{g}{\rho0}\frac{\partial\rho}{\partial z} \quad (20)$$

A_1, A_2, B_1 and B_2 are constants that determine the ratios of various turbulence length scales to the turbulence macro-scale l. The turbulence closure assumes that all turbulence length scales are proportional to one another.

S_M and S_H are functions of G_H, which is in turn a function of the buoyancy gradient. The term multiplying q^3/B_1 in Equation (14) is a wall proximity function inserted empirically to assure log-law behavior near solid boundaries and L is given:

$$L^{-1}=z^{-1}+\left(D+z\right)^{-1} \quad (21)$$

where D is the depth of the fluid column.

$$(A_1, A_2, B_1, B_2, C_1, E_1, E_2, E_3) = (0.92,\ 0.74,\ 16.6,\ 10.1,\ 0.08,\ 1.8,\ 1.8,\ 1.33) \quad (22)$$

Terms C_1, E_1, E_2 and E_3 are empirical constants determined by appealing to well-known laboratory experiments on turbulence, as are constants A_1, A_2, B_1 and B_2.

κ is the well-known von Karman constant (= 0.4) that occurs in the log-law governing the velocity profile adjacent to a boundary in a turbulent boundary layer.

3. Free Surface Boundary Conditions

Free surface is a material surface:

$$w = \frac{\partial \eta}{\partial t} + u_1 \frac{\partial \eta}{\partial x_1} + u_2 \frac{\partial \eta}{\partial x_2} \quad (23)$$

where $z = \eta(x_1, x_2)$.

Momentum and buoyancy fluxes (comprised of heat, salt and other fluxes) at the free surface are the driving mechanisms for the ocean and must satisfy following equations:

$$K_M \left(\frac{\partial u_1}{\partial z}, \frac{\partial u_2}{\partial z} \right) = \frac{1}{\rho_0} (\tau_{01}, \tau_{02}) \quad (24.1)$$

$$K_M \left(\frac{\partial \Theta}{\partial z}, \frac{\partial S_i}{\partial z} \right) = \frac{1}{\rho_0} \left(\overline{Q_H}, \overline{Q_{S_i}} \right) \quad (24.2)$$

where τ_{01} and τ_{02} are the wind stress components, and $\overline{Q\mathrm{H}}$, $\overline{Q_{S_i}}$, ... are the heat and salt and other pollutant fluxes at the surface. $\overline{Q\mathrm{H}}$ is the result of energy balance at the ocean surface involving the impinging short and long wave solar radiation, the back radiation from the ocean, and the sensible latent heat fluxes from the ocean to the atmosphere:

$$\overline{Q_H} = \overline{\beta}\left(1 - \overline{\alpha}\right) S_W + L_W - \varepsilon \overline{\sigma} \overline{T_S^4} - H_S - H_L \quad (25)$$

S_W is the short-wave solar radiation flux, L_W is the longwave solar radiation flux, $\overline{\alpha}$ is the albedo, ε the emissivity of the ocean surface, $\overline{\sigma}$ is the Stefan-Boltzmann constant, T_S is the sea surface temperature, and H_S and H_L are the sensible and latent heat fluxes. If $\overline{\beta}$ is put equal to unity, then Q_S in Equation (11) must be put to zero, implying that all the incident shortwave radiation is absorbed at the surface and there is no penetrative heating of the ocean. The salt flux $\overline{Q_S}$ at the ocean surface is:

$$\overline{Q_S} = S_s \left(\dot{E} - \dot{P} \right) \quad (26)$$

Surface salinity E is of course related to the latent heat flux H_L.

If the sea surface temperature and salinity are known, then an alternative to Equation (26) would be:

$$\left(\Theta, S_i \right) = \left(T_S, (S_i)_S \right) \quad (27)$$

Another alternative is to damp the surface values of Θ and S_i to the sea surface values with a time lag t_l:

$$\frac{\partial}{\partial t} \left(\Theta, S_i \right) = -\frac{1}{t_l} \left[\left(\Theta - T_S \right), \left(S_i - (S_i)_S \right) \right] \quad (28)$$

Conditions (27) and (28) are most often used in climatologically simulations, while Equation (26) is useful for driving the ocean with synoptic momentum and buoyancy fluxes. The conditions on q^2 and l at the free surface are:

$$q^2 = B_1^{2/3} u_{*0}^2 \ \text{ and } \ l = 0 \quad (29.1)$$

$$u_{*0} = \left[\left(\tau_{01}^2 + \tau_{02}^2 \right) / \rho_{01}^2 \right]^{1/4} \quad (29.2)$$

where u_{*0} is the friction velocity at the free surface.

4. Ocean Bottom Boundary Conditions

At the ocean bottom, $z = -H$, there can be no flux of heat, salt or other fluxes:

$$\left(\frac{\partial \Theta}{\partial z}, \frac{\partial S_i}{\partial z} \right)_b = \left(0, 0_i \right) \quad (30)$$

where the subscript b denotes the lower boundary. There can also be no mass flux through the bottom leading to:

$$\omega = -u_{1b} \frac{\partial H}{\partial x_1} - u_{2b} \frac{\partial H}{\partial x_2} \quad (31)$$

The remaining boundary conditions are:

$$K_M \left(\frac{\partial u_1}{\partial z}, \frac{\partial u_2}{\partial z} \right) = \frac{1}{\rho_0} (\tau_{b1}, \tau_{b2}) \quad (32)$$

$$q^2 = B_1^{2/3} u_{*b}^2 \ \text{ and } \ l = 0 \quad (33)$$

where τ_{b1} and τ_{b2} are the shear stress components at the bottom and $u_{*b} = [(\tau_{b1}^2 + \tau_{b2}^2) / \rho_{01}^2]^{1/4}$ is the friction velocity at the bottom. The bottom stresses are determined by matching the velocities u_{1b} and u_{2b} at the lowest grid point z_b to a logarithmic law of the wall:

$$\left(\tau_{b1}, \tau_{b2} \right) = \rho_0 C_D \left[u_{1b}^2 + u_{2b}^2 \right]^{1/2} \left(u_{1b}, u_{2b} \right) \quad (34)$$

where the drag coefficient C_D is determined from log-law:

$$C_D = \left[\frac{1}{\kappa}\ln\left(\frac{H+z_b}{z_0}\right)\right]^{-2} \tag{35}$$

where z_0 is the roughness scale, of the order of a centimeter or so for moderately rough bed.

Equations (34) and (35) assume that the lowest grid point is in the log layer. If the model vertical resolution is not adequate to satisfy this condition, the drag coefficient is set to a value of 0.0025 which results in a conventional quadratic drag law. The model algorithm chooses the larger of this value and the value given by Equation (35) in order to satisfy this prescription.

5. Lateral Boundary Conditions

For a closed basin, the lateral boundary conditions are straightforward. The conditions of zero mass, momentum, heat, salt and turbulence fluxes must be satisfied at a solid lateral boundary. However, at open boundaries, the influence of the region exterior to the model domain must be specified.

When there is inflow, Θ and S_i need to be prescribed, whilst for outflow, Θ and S_i need to be adverted out:

$$\frac{\partial}{\partial t}(\Theta, S_i) + u_n \frac{\partial}{\partial n}(\Theta, S_i) = 0 \tag{36}$$

where n denotes the coordinate normal to the lateral boundary. In relation to q^2 and I, it is possible to ignore any advection at the lateral boundaries without affecting the overall accuracy.

Prescription of mass and momentum conditions at an open boundary are more difficult since these are really a function of the interaction with the exterior domain and unknown a priori modeling of a limited region. Nevertheless, inflow and outflow must somehow be specified as functions of time. The most important requirement is to satisfy the mass balance. Thus open boundary conditions must be specified such that there is no net mass increase over a specified period of time. For tidal (or barotropic) calculations the free surface elevation [η(t)] may be prescribed on the boundary. Often a Summerfield radiation condition is of the form:

$$\frac{\partial \phi}{\partial t} + c\frac{\partial \phi}{\partial \eta} = 0 \tag{37}$$

where ϕ is any quantity such as η, u_1, … and c is the phase speed of a disturbance approaching the boundary from the interior of the domain.

6. Transformation from Cartesian to Sigma Coordinate

As discussed earlier, a topographically conformal vertical coordinate system has many advantages in dealing with an ocean basin with wide disparities depth, although this has its own drawbacks. We will now transform the governing equations from z coordinate to Sigma-coordinate by following equations (Figure 1):

$$\sigma = \frac{z-\eta}{\mathrm{H}+\eta} \tag{38}$$

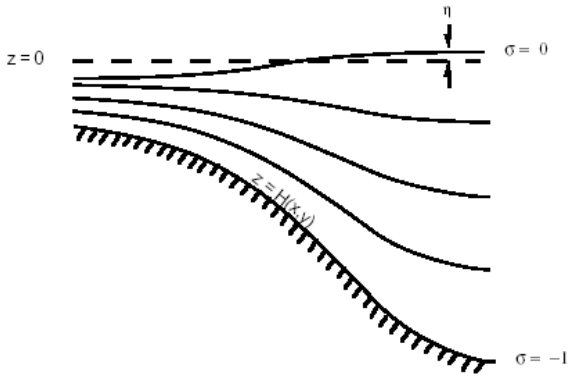

Figure 1. Sigma coordinate system.

Formally, we transform the equations from a (x_1, x_2, z, t) coordinate system to the (x_1, x_2, σ, t) system, where x_1, x_2, and t are not changed. Let t be a dependent variable that denotes any quantity represented from ocean properties. Then the derivatives of this quantity are related as follows (Mellor, 1998):

$$\frac{\partial \phi}{\partial x_1} = \frac{\partial \phi}{\partial x_1} - \frac{\partial \phi}{\partial \sigma}\left(\frac{\sigma}{D}\frac{\partial D}{\partial x_1} + \frac{1}{D}\frac{\partial \eta}{\partial x_1}\right) \tag{39}$$

$$\frac{\partial \phi}{\partial x_2} = \frac{\partial \phi}{\partial x_2} - \frac{\partial \phi}{\partial \sigma}\left(\frac{\sigma}{D}\frac{\partial D}{\partial x_2} + \frac{1}{D}\frac{\partial \eta}{\partial x_2}\right) \tag{40}$$

$$\frac{\partial \phi}{\partial z} = \frac{1}{D}\frac{\partial \phi}{\partial \sigma} \tag{41}$$

$$\frac{\partial \phi}{\partial t} = \frac{\partial \phi}{\partial t} - \frac{\partial \phi}{\partial \sigma}\left(\frac{\sigma}{D}\frac{\partial D}{\partial t} + \frac{1}{D}\frac{\partial \eta}{\partial t}\right) \tag{42}$$

Substituting the above statements in equations of continuity, momentum, temperature, salinity, density and turbulence in Section (2) results in the follows:

$$\frac{\partial \eta}{\partial t} + \frac{1}{h_1 h_2}\left[\frac{\partial}{\partial x_1}(h_2 u_1 D) + \frac{\partial}{\partial x_2}(h_1 u_2 D)\right] + \frac{\partial \overline{w}}{\partial \sigma} = 0 \tag{43}$$

$$\frac{\partial}{\partial t}(u_1 D) + \frac{1}{h_1 h_2}\left[\frac{\partial}{\partial x_1}(h_2 u_1^2 D) + \frac{\partial}{\partial x_2}(h_1 u_1 u_2 D)\right] + \frac{\partial}{\partial \sigma}(\overline{w u_1}) + \frac{u_1 u_2 D}{h_1 h_2}\frac{\partial h_1}{\partial x_2} - \frac{u_2^2 D}{h_1 h_2}\frac{\partial h_2}{\partial x_1} - f u_2 D = -DP_1 + \frac{\partial}{\partial \sigma}\left(\frac{K_M}{D}\frac{\partial u_1}{\partial \sigma}\right) + DF_1 \tag{44}$$

$$\frac{\partial}{\partial t}(u_2 D)+\frac{1}{h_1 h_2}\left[\frac{\partial}{\partial x_1}(h_2 u_1 u_2 D)\frac{\partial}{\partial x_2}\left(h_1 u_2^2 D\right)\right]+\frac{\partial}{\partial \sigma}\left(\overline{w}u_2\right)$$
$$+\frac{u_1 u_2 D}{h_1 h_2}\frac{\partial h_2}{\partial x_1}-\frac{u_1^2 D}{h_1 h_2}\frac{\partial h_1}{\partial x_2}-fu_1 D=-D\mathrm{P}_2+\frac{\partial}{\partial \sigma}\left(\frac{K_M}{D}\frac{\partial u_2}{\partial \sigma}\right)+DF_2 \tag{45}$$

$$\frac{\partial}{\partial t}(\Theta D)+\frac{1}{h_1 h_2}\left[\frac{\partial}{\partial x_1}(h_2 u_1 \Theta D)+\frac{\partial}{\partial x_2}(h_1 u_2 \Theta D)\right]+\frac{\partial}{\partial \sigma}\left(\overline{w}\Theta\right)$$
$$=\frac{\partial}{\partial \sigma}\left(\frac{K_H}{D}\frac{\partial \Theta}{\partial \sigma}\right)+DF_\Theta \tag{46}$$

$$\frac{\partial}{\partial t}(S_i D)+\frac{1}{h_1 h_2}\left[\frac{\partial}{\partial x_1}(h_2 u_1 S_i D)+\frac{\partial}{\partial x_2}(h_1 u_2 S_i D)\right]+\frac{\partial}{\partial \sigma}\left(\overline{w}S_i\right)$$
$$=\frac{\partial}{\partial \sigma}\left(\frac{K_H}{D}\frac{\partial S_i}{\partial \sigma}\right)+DF_{S_i} \tag{47}$$

$$\frac{\partial}{\partial t}\left(q^2 D\right)+\frac{1}{h_1 h_2}\left[\frac{\partial}{\partial x_1}\left(h_2 u_1 q^2 D\right)+\frac{\partial}{\partial x_2}\left(h_1 u_2 q^2 D\right)\right]$$
$$+\frac{\partial}{\partial \sigma}\left(\overline{w}q^2\right)=\frac{\partial}{\partial \sigma}\left(\frac{K_p}{D}\frac{\partial q^2}{\partial \sigma}\right)+\frac{2K_M}{D}\left[\left(\frac{\partial u_1}{\partial \sigma}\right)^2+\left(\frac{\partial u_2}{\partial \sigma}\right)^2\right] \tag{48}$$
$$+2K_H\frac{g}{\rho}\frac{\partial \rho}{\partial \sigma}-\frac{2q^3 D}{B_1 l}DF_q$$

$$\frac{\partial}{\partial t}\left(q^2 lD\right)+\frac{1}{h_1 h_2}\left[\frac{\partial}{\partial x_1}\left(h_2 u_2 q^2 lD\right)+\frac{\partial}{\partial x_2}\left(h_1 u_2 q^2 lD\right)\right]$$
$$+\frac{\partial}{\partial \sigma}\left(\overline{w}q^2 l\right)=\frac{\partial}{\partial \sigma}\left[\frac{K_q}{D}\frac{\partial}{\partial \sigma}\left(q^2 l\right)\right]+K_M E_1\frac{l}{D}\left[\left(\frac{\partial u_1}{\partial \sigma}\right)^2\right. \tag{49}$$
$$\left.+\left(\frac{\partial u_2}{\partial \sigma}\right)^2\right]+K_H E_3 l\frac{g}{\rho}\frac{\partial \rho}{\partial \sigma}-\frac{q^3 D}{B_1}\left[1+E_2\left(\frac{l}{\kappa L}\right)^2\right]+DF_l$$

$$\overline{w}=w-u_1\sigma\frac{\partial D}{\partial x_1}+\frac{\partial \eta}{x_1}-u_2\sigma\frac{\partial D}{\partial x_2}+\frac{\partial \eta}{\partial x_2}-\left(\sigma\frac{\partial D}{\partial t}+\frac{\partial \eta}{\partial t}\right) \tag{50}$$

where $\overline{w}$ is a pseudo-vertical velocity in the new coordinate system given by:

$$\overline{w}=0 \quad \text{at} \quad \sigma=0 \quad \text{and} \quad \sigma=-1 \tag{51}$$

The pressure gradient terms are:

$$DP_1=\frac{D}{\rho 0}\frac{\partial p_a}{\partial x_1}+\rho D\frac{\partial \eta}{\partial \chi_1}+\frac{gD^2}{\rho 0}\left[\frac{\partial}{\partial x_1}\int_\sigma^0 \rho d\sigma'\right.$$
$$\left.-\rho\left(\frac{\sigma}{D}\frac{\partial D}{\partial x_1}+\frac{1}{D}\frac{\partial \eta}{\partial x_1}\right)\right]-\frac{gD}{\rho 0}\frac{\partial D}{\partial x_1}\int_\sigma^0 \sigma'\frac{\partial \rho}{\partial \sigma'}d\sigma' \tag{52}$$

$$DP_2=\frac{D}{\rho 0}\frac{\partial p_a}{\partial x_2}+\rho D\frac{\partial \eta}{\partial x_2}+\frac{gD^2}{0}\left[\frac{\partial}{\partial x_2}\int_\sigma^0 \rho d\sigma'\right.$$
$$\left.-\rho\left(\frac{\sigma}{D}\frac{\partial D}{\partial x_2}+\frac{1}{D}\frac{\partial \eta}{\partial x_2}\right)\right]-\frac{gD}{\rho 0}\frac{\partial D}{\partial x_2}\int_\sigma^0 \sigma'\frac{\partial \rho}{\partial \sigma'}d\sigma' \tag{53}$$

The horizontal viscosity terms are:

$$DF_1=\frac{1}{h_1 h_2}\left\{\frac{\partial}{\partial x_1}(h_2\tau_{11})-h_2\frac{\partial}{\partial \sigma}\left[\left(\frac{\sigma}{D}\frac{\partial D}{\partial x_2}+\frac{1}{D}\frac{\partial \eta}{\partial x_2}\right)\tau_{11}\right]\right\}$$
$$+\frac{\partial}{\partial x_2}\left\{h_1\tau_{21}-h_1\frac{\partial}{\partial \sigma}\left[\left(\frac{\sigma}{D}\frac{\partial D}{\partial x_2}+\frac{1}{D}\frac{\partial \eta}{\partial x_2}\right)\tau_{21}\right]+\tau_{21}\frac{\partial h_1}{\partial x_2}-\tau_{22}\frac{\partial h_2}{\partial x_1}\right\} \tag{54}$$

$$DF_2=\frac{1}{h_1 h_2}\left\{\frac{\partial}{\partial x_1}(h_2\tau_{12})-h_2\frac{\partial}{\partial \sigma}\left[\left(\frac{\sigma}{D}\frac{\partial D}{\partial x_1}+\frac{1}{D}\frac{\partial \eta}{\partial x_1}\right)\tau_{12}\right]\right\}$$
$$+\frac{\partial}{\partial x_2}\left\{(h_1\tau_{22})-h_1\frac{\partial}{\partial \sigma}\left[\left(\frac{\sigma}{D}\frac{\partial D}{\partial x_2}+\frac{1}{D}\frac{\partial \eta}{\partial x_2}\right)\tau_{22}\right]+\tau_{12}\frac{\partial h_2}{\partial x_1}-\tau_{11}\frac{\partial h_1}{\partial x_2}\right\} \tag{55}$$

$$\tau_{11}=2A_M\left\{\frac{1}{h_1}\left[\frac{\partial}{\partial x_1}(\mu_1 D)-\frac{\partial}{\partial \sigma}\left[\mu_1\left(\sigma\frac{\partial D}{\partial x_1}+\frac{\partial \eta}{\partial \chi_1}\right)\right]\right]+\frac{\mu_2 D}{h_1 h_2}\frac{\partial h_1}{\partial x_2}\right\} \tag{56}$$

$$\tau_{12}=2\mathrm{A}_\mathrm{M}\left\{\frac{h_1}{h_2}\left[\frac{\partial}{\partial x_2}\left(\frac{\mu_1 D}{h_1}\right)-\frac{1}{h_1}\frac{\partial}{\partial \sigma}\left[\left(\sigma\frac{\partial D}{\partial x_2}+\frac{\partial \eta}{\partial x_2}\right)\mu_1\right]\right]\right\}$$
$$+\frac{h_2}{h_1}\left[\frac{\partial}{\partial x_1}\left(\frac{\mu_2 D}{h_2}\right)-\frac{1}{h_2}\frac{\partial}{\partial \sigma}\left[\left(\sigma\frac{\partial D}{\partial x_1}+\frac{\partial \eta}{\partial x_1}\right)\mu_2\right]\right] \tag{57}$$

$$\tau_{22}=2A_M\left\{\frac{1}{h_2}\left[\frac{\partial}{\partial x_2}(\mu_2 D)-\frac{\partial}{\partial \sigma}\left(\mu_2\left(\sigma\frac{\partial D}{\partial x_2}+\frac{\partial \eta}{\partial x_2}\right)\right)\right]\frac{\mu_1 D}{h_1 h_2}\frac{\partial h_2}{\partial x_1}\right\} \tag{58}$$

The horizontal diffusion terms are:

$$DF_\Theta=\frac{1}{h_1 h_2}\left\{\frac{\partial}{\partial x_1}(h_2 q_1)-h_2\frac{\partial}{\partial \sigma}\left[\left(\frac{\sigma}{D}\frac{\partial D}{\partial x_1}+\frac{1}{D}\frac{\partial \eta}{\partial x_1}\right)q_1\right]\right\}$$
$$+\frac{\partial}{\partial x_2}(h_1 q_2)-h_1\frac{\partial}{\partial \sigma}\left[\left(\frac{\sigma}{D}\frac{\partial D}{\partial x_2}+\frac{1}{D}\frac{\partial \eta}{\partial x_2}\right)q_2\right] \tag{59}$$

$$q_1=A_H\frac{1}{h_1}\left\{\frac{\partial}{\partial x_1}(\Theta D)-\frac{\partial}{\partial \sigma}\left[\left(\sigma\frac{\partial D}{\partial x_1}+\frac{\partial \eta}{\partial x_1}\right)\Theta\right]\right\} \tag{60}$$

$$q_2=A_H\frac{1}{h_2}\left\{\frac{\partial}{\partial x_2}(\Theta D)-\frac{\partial}{\partial \sigma}\left[\left(\sigma\frac{\partial D}{\partial x_2}+\frac{\partial \eta}{\partial x_2}\right)\Theta\right]\right\} \tag{61}$$

$$DF_{S_i} = \frac{1}{h_1 h_2}\left\{\frac{\partial}{\partial x_1}(h_2 q_1) - h_2\frac{\partial}{\partial\sigma}\left[\left(\frac{\sigma}{D}\frac{\partial D}{\partial x_1}+\frac{1}{D}\frac{\partial\eta}{\partial x_1}\right)q_1\right]\right\} + \frac{\partial}{\partial x_2}(h_1 q_2) - h_1\frac{\partial}{\partial\sigma}\left[\left(\frac{\sigma}{D}\frac{\partial D}{\partial x_2}+\frac{1}{D}\frac{\partial\eta}{\partial x_2}\right)q_2\right] \quad (62)$$

$$q_1 = A_H\frac{1}{h_1}\left\{\frac{\partial}{\partial x_1}(S_i D) - \frac{\partial}{\partial\sigma}\left[\left(\sigma\frac{\partial D}{\partial x_1}+\frac{\partial\eta}{\partial x_1}\right)S_i\right]\right\} \quad (63)$$

$$q_2 = A_H\frac{1}{h_2}\left\{\frac{\partial}{\partial x_2}(S_i D) - \frac{\partial}{\partial\sigma}\left[\left(\sigma\frac{\partial D}{\partial x_2}+\frac{\partial\eta}{\partial x_2}\right)S_i\right]\right\} \quad (64)$$

$$DF_{S_i} = \frac{1}{h_1 h_2}\left\{\frac{\partial}{\partial x_1}(h_2 q_1) - h_2\frac{\partial}{\partial\sigma}\left[\left(\frac{\sigma}{D}\frac{\partial D}{\partial x_1}+\frac{1}{D}\frac{\partial\eta}{\partial x_1}\right)q_1\right]\right\} + \frac{\partial}{\partial x_2}(h_1 q_2) - h_1\frac{\partial}{\partial\sigma}\left[\left(\frac{\sigma}{D}\frac{\partial D}{\partial x_2}+\frac{1}{D}\frac{\partial\eta}{\partial x_2}\right)q_2\right] \quad (65)$$

$$q_1 = A_H\frac{1}{h_1}\left\{\frac{\partial}{\partial x_1}(\psi_i D) - \frac{\partial}{\partial\sigma}\left[\left(\sigma\frac{\partial D}{\partial x_1}+\frac{\partial\eta}{\partial x_1}\right)\psi_i\right]\right\} \quad (66)$$

$$q_2 = A_H\frac{1}{h_2}\left\{\frac{\partial}{\partial x_2}(\psi_i D) - \frac{\partial}{\partial\sigma}\left[\left(\sigma\frac{\partial D}{\partial x_2}+\frac{\partial\eta}{\partial x_2}\right)\psi_i\right]\right\} \quad (67)$$

$$DF_q = \frac{1}{h_1 h_2}\left\{\frac{\partial}{\partial x_1}(h_2 q_1) - h_2\frac{\partial}{\partial\sigma}\left[\left(\frac{\sigma}{D}\frac{\partial D}{\partial x_1}+\frac{1}{D}\frac{\partial\eta}{\partial x_1}\right)q_1\right]\right\} + \frac{\partial}{\partial x_2}(h_1 q_2) - h_1\frac{\partial}{\partial\sigma}\left[\left(\frac{\sigma}{D}\frac{\partial D}{\partial x_2}+\frac{1}{D}\frac{\partial\eta}{\partial x_2}\right)q_2\right] \quad (68)$$

$$q_1 = A_H\frac{1}{h_1}\left\{\frac{\partial}{\partial x_1}(q^2 D) - \frac{\partial}{\partial\sigma}\left[\left(\sigma\frac{\partial D}{\partial x_1}+\frac{\partial\eta}{\partial x_1}\right)q^2\right]\right\} \quad (69)$$

$$q_2 = A_H\frac{1}{h_2}\left\{\frac{\partial}{\partial x_2}(q^2 D) - \frac{\partial}{\partial\sigma}\left[\left(\sigma\frac{\partial D}{\partial x_2}+\frac{\partial\eta}{\partial x_2}\right)q^2\right]\right\} \quad (70)$$

$$DF_l = \frac{1}{h_1 h_2}\left\{\frac{\partial}{\partial x_1}(h_2 q_1) - h_2\frac{\partial}{\partial\sigma}\left[\left(\frac{\sigma}{D}\frac{\partial D}{\partial x_1}+\frac{1}{D}\frac{\partial\eta}{\partial x_1}\right)q_1\right]\right\} + \frac{\partial}{\partial x_2}(h_1 q_2) - h_1\frac{\partial}{\partial\sigma}\left[\left(\frac{\sigma}{D}\frac{\partial D}{\partial x_2}+\frac{1}{D}\frac{\partial\eta}{\partial x_2}\right)q_2\right] \quad (71)$$

$$q_1 = A_H\frac{1}{h_1}\left\{\frac{\partial}{\partial x_1}(q^2 l D) - \frac{\partial}{\partial\sigma}\left[\left(\sigma\frac{\partial D}{\partial x_1}+\frac{\partial\eta}{\partial x_1}\right)q^2 l\right]\right\} \quad (72)$$

$$q_2 = A_H\frac{1}{h_2}\left\{\frac{\partial}{\partial x_2}(q^2 l D) - \frac{\partial}{\partial\sigma}\left[\left(\sigma\frac{\partial D}{\partial x_2}+\frac{\partial\eta}{\partial x_2}\right)q^2 l\right]\right\} \quad (73)$$

7. Design of the Unstructured Grids

The horizontal grids comprise unstructured triangular cells which similar to the finite-element method. The horizontal numerical computational domain is subdivided into non-overlapping cells. An unstructured triangle comprises three nodes, a centroid, and three sides (Figure 2). The irregular bottom slope is represented using a Sigma coordinate transformation.

Delaunay Triangulation method is used for the horizontal grids and Laplacian Smoothing method is subsequently used for mesh smoothing. Delaunay Triangulation is the most widely used triangulation method in unstructured mesh generation. It is one of the fastest triangulation methods with relatively easier implementation, giving excellent results for most applications.

In Delaunay Triangulation, the boundary triangulation is not difficult. Although it should be noted that placing the interior points at inappropriate places may result in bad meshes, even though the Delaunay criterion is satisfied.

8. Numerical Method

The finite-difference method is the simplest discrete scheme with the advantage of computational efficiency. Introducing an orthogonal or non-orthogonal curvilinear coordinate transformation into a finite-difference model can provide a moderate fitting of coastal boundaries, but these transformations are incapable of resolving the highly irregular estuarine geometries characteristic of numerous barrier islands and tidal creek complexes (Blumberg, 1994; Chen et al., 2001; Chen et al., 2003). The most important advantage of finite-element method is its geometric flexibility. Triangular meshes at an arbitrary size are used in this method which provides an accurate fitting of the irregular coastal boundary.

The P-type finite-element method (Maday and Patera, 1989) or discontinuous Galerkin method (Reed and Hill, 1973; Cockburn et al., 1990) has been introduced into the updated finite-element model to improve computational accuracy and efficiency. The finite-volume method has been received considerable attention in the numerical computation of fluid dynamics (Dick, 1994). The dynamics of oceanography comply with conservation laws. The governing equations of oceanic motion and water masses are expressed by the conservation of momentum, mass, and energy in a unit volume. When the equations are solved numerically, these laws cannot always be guaranteed, especially in situations with sharp thermo clines or discontinuous flow. Unlike the differential form, the finite volume method discretizes the integral form of the equations making it easier to comply with the conservation laws.

Since these integral equations can be solved numerically by the flux calculation used in the finite-difference method over an arbitrarily sized triangular mesh (like those in a finite-element method), the finite-volume method seems to combine the best attributes of the finite-difference method for simple discrete computational efficiency and the finite-element method for geometric flexibility.

A three-dimensional (3D), unstructured grid, primitive equation, finite-volume ocean circulation model can be considered as a new approach in the oceanographic community. Also some efforts have been made to develop a finite-volume formulation of the two-dimensional, barotropic shallow water equations (Ward, 2000). The MIT General Circulation model (Marshall, et al., 1997a and 1997b) was the first 3D finite-volume ocean model. However, since this model currently relies on rectangular structure grids for horizontal discretization, it is not suitable to be used for coastal ocean and estuarine domains with complicated geometries.

Due to the special features and nature of this subject, the method of unstructured grids has been selected to use in this research. The numerical model solves for prognostic variables η, u_1, u_2, Θ, S, …, q^2 and l as a function of time, starting from a specified set of initial conditions, forced by the wind stress and buoyancy flux at the ocean surface, and prescribed transports at open lateral boundaries. These prognostic variables are staggered not only in the horizontal, but also in the vertical direction. In fact, q, l, w, K_M and K_H are located at σ levels, while variables such as u_1, u_2, Θ, S, and ρ are staggered in vertical, located between two corresponding σ levels. Note that w, q, l, Θ, S_i, ρ, K_M and K_H are located at the nodes of the grid, whereas u_1, u_2 are staggered horizontally as described before. Shear stresses τ_1 and τ_2 are staggered in the horizontal, located at sigma levels (Figure 2).

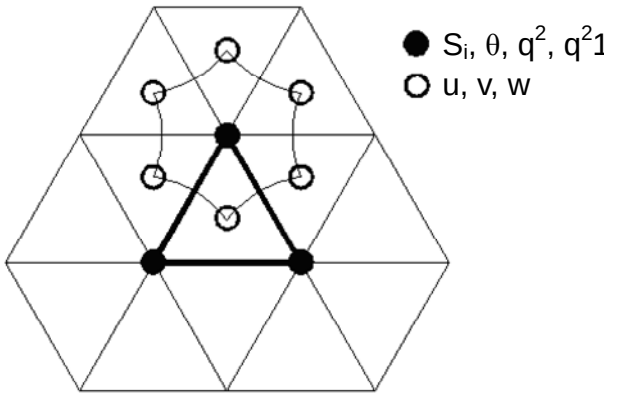

Figure 2. Locations of the parameters on the mesh.

The governing differential equations are in flux-conservative form, hence mass and energy are conserved when the equations are discretized. Therefore, finite volume approximations can be derived by use of a control volume approach.

The external mode equations are also cast in similar finite volume forms, which are omitted for brevity. The external and internal mode of finite volume equations are solved in a split-mode method to obtain solutions for the prognostic quantities as a function of time. The external mode is solved using explicit difference techniques. The internal mode equations are solved implicitly in the vertical direction and explicitly in the horizontal. The finite volume equations for the internal mode are cast as a tri-diagonal matrix form, which are then solved using well-known techniques such as Thomas tri-diagonal algorithm. Close synchronization between external and internal modes, is ensured by utilizing the internal mode bottom friction and also the density field pressure gradient component, in the external mode. In turn, the external mode supplies the internal mode with the sea surface elevation and vertically averaged currents information. This interaction takes place at each internal time step. The procedure then is to start with one external mode calculation and then pass on the needed information to the internal mode and take one time step with it. The internal mode then passes on the needed information to the external mode and the entire process is repeated until the end of the calculation is reached. The continuity equations for numerical solution are as follows:

$$(h_1\delta x_1)(h_2\delta x_2)\frac{\partial \eta}{\partial t}+\frac{\partial}{\partial x_1}(h_2\delta x_2.u_1D)\delta x_1+\frac{\partial}{\partial x_2}(h_1\delta x_1.u_2D)\delta x_2=0 \tag{74}$$

$$\iint\left[(h_1\delta x_1)(h_2\delta x_2)\frac{\partial \eta}{\partial t}+\frac{\partial}{\partial x_1}(h_2\delta x_2.u_1D)\delta x_1+\frac{\partial}{\partial x_2}(h_1\delta x_1.u_2D)\delta x_2\right] dx_1dx_2=0 \tag{75}$$

$$(h_1\delta x_1)(h_2\delta x_2)\frac{\partial \eta}{\partial t}+\frac{\partial}{\partial x_1}(h_2\delta x_2.u_1D)\delta x_1 +\frac{\partial}{\partial x_2}(h_1\delta x_1.u_2D)\delta x_2+(h_1\delta x_1)(h_2\delta x_2)\frac{\partial w}{\partial \sigma}=0 \tag{76}$$

$$\iiint\left[(h_1\delta x_1)(h_2\delta x_2)\frac{\partial \eta}{\partial t}+\frac{\partial}{\partial x_1}(h_2\delta x_2.u_1D)\delta x_1 +\frac{\partial}{\partial x_2}(h_1\delta x_1.u_2D)\delta x_2+(h_1\delta x_1)(h_2\delta x_2)\frac{\partial w}{\partial \sigma}\right]dx_1dx_2d\sigma=0 \tag{77}$$

Also, the momentum equations for numerical solution are obtained from (44):

$$(h_1\delta x_1)(h_2\delta x_2)\frac{\partial}{\partial t}(u_1D)+\frac{\partial}{\partial x_1}(u_1^2D\cdot h_2\delta x_2)\delta x_1+\frac{\partial}{\partial x_2}(u_1u_2D \cdot h_1\delta x_1)\delta x_2+u_1u_2D\frac{\partial}{\partial x_2}(h_1\delta x_1)\cdot\delta x_2-u_1^2D\cdot\frac{\partial}{\partial x_1}(h_2\delta x_2)\cdot\delta x_1 -(h_1\delta x_1)(h_2\delta x_2)fu_2D+(h_1\delta x_1)(h_2\delta x_2)\frac{\partial}{\partial \sigma}(wu_1)=\ldots \tag{78}$$

$$\Delta x_1\cdot\Delta x_2\delta_t(u_1D)+\Delta x_1(u_1^2D\cdot\Delta x_2)+\Delta x_2(u_1u_2D\cdot\Delta x_1) -\Delta x_1\cdot\Delta x_2\left\{f+\frac{1}{\Delta x_1\cdot\Delta x_2}\left[u_2\Delta x_1(\Delta x_2)-u_1\Delta x_2(\Delta x_1)\right]\right\}u_2D +\Delta x_1\Delta x_2\cdot\delta_\sigma(wu_1)=\ldots \tag{79}$$

$$\Delta x_1\cdot\Delta x_2\cdot\delta_t(u_2D)+\Delta x_1(u_1u_2D\Delta x_2)+\Delta x_2(u_2^2D\Delta x_1) +\Delta x_1\cdot\Delta x_2\cdot\tilde{f}u_1D+\Delta x_1\cdot\Delta x_2\cdot\delta_\sigma(wu_2)=\ldots \tag{80}$$

$$\tilde{f} = f + \frac{1}{\Delta x_1 \cdot \Delta x_2}\left[u_2 \Delta x_1(\Delta x_2) - u_1 \Delta x_2(\Delta x_1)\right] \quad (81)$$

9. Description of Procedures

The model has been developed in two separated parts in order to simplify the simulations. The first part is devoted to simulate the simple geometries, and the second part devoted to simulate the southern Caspian Sea which has more complicated geometry.

First part of geometries, which is not complicated, is used for simple validation of the equations. We assume four simple geometries in rectangular shapes (Figure 3). In Figures 3(a) and 3(b), the domain shapes are different. In Figures 3(c) and 3(d), we assume two different islands configurations.

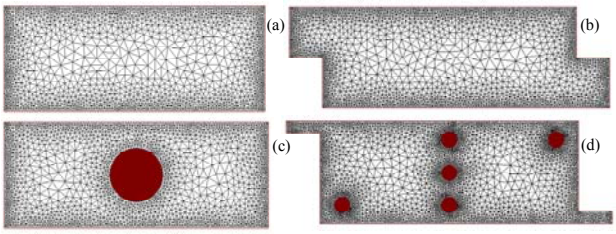

Figure 3. Grid mesh generation for different types of geometries to test model verification: (a) Rectangular Shape; (b) Semi Rectangular Shape; (c) Rectangular Shape with One Island; and (d) Semi Rectangular Shape with Five Island.

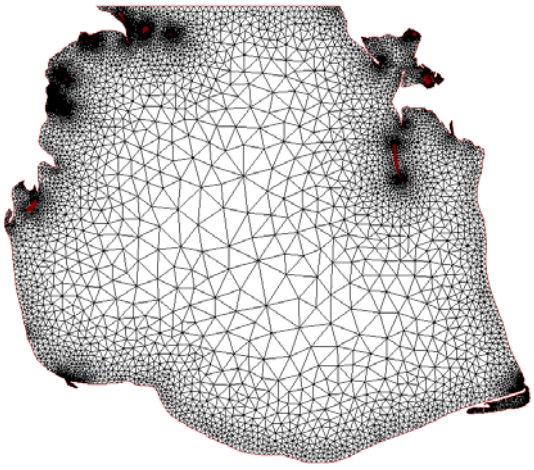

Figure 4. Southern Caspian Sea Domain.

These geometries (a, b, c, d), with 50 km width, 20 km length and constant depth of 16m, are located in Noshahr in south of Caspian Sea. It should be noted that the effects of Coriolis force are used in calculations.

For the second part (Figure 4), we assume the Caspian Sea in its real location (latitude and longitude):

At first, unstructured grid, finite-volume, ocean circulation model is applied in geometries mentioned in Figure 3. The procedure has two parts:

I) Circulation,
II) Pollutant distribution.

For both parts, we assume water is stationary, there is no tidal elevation, precipitation and evaporation are equal, and distributed temperature and pollutant are constant. Also the initial temperature of water and rivers input is 20 °C.

In part (I), different conditions are supposed as below:

I-1) Coriolis force,
I-2) Wind force,
I-3) Both Coriolis and wind forces,
I-4) River inputs,
I-5) Conditions (I-3) and (I-4) together.

For part (II), the conditions are:

II-1) Pollutant from rivers,
II-2) Pollutant from rivers with Coriolis force,
II-3) Pollutant from rivers with wind force,
II-4) Conditions (II-2) and (II-3) together,
II-5) Condition (II-4) with many pollutant sources.

10. Simulation Results

In this section, from all simulations, we select some typical ones to illustrate the results. All simulations are applied to third domain of (Figure 3c). In Figure 5, the condition (I-1) is applied to the discussed domain, with $\sigma = 1$ and time duration of two weeks. In Figure 6, the condition (I-4) with $\sigma = 1$ and time duration of two weeks is applied. The flow rate for two rivers (Northwest-input, Southeast-output) is 5 m^3/s. Result of experimental run of condition (I-5) with time duration of two weeks, two 5 m^3/s river inputs (northwest and southeast), 1 m/s north wind and $\sigma = 1$ is in Figure 7. Result of experimental run of condition (II-4) with time duration of two weeks, same conditions for river inputs and wind as previous run, 30 ppm salinity rivers contain (domain does not have initial salinity) and $\sigma = 1$ is shown in Figure 8. Result of experimental run of condition (II-5) with time duration of one week, three 5 m^3/s river inputs, three 15, 30, 40 ppm multi-pollutant sources (the domain has initial pollutants of 10, 25, 35 ppm), 8 m/s west to east wind and $\sigma = 1$ is shown in Figure 9. If all input sources are closed, after one week, the simulation result is as shown in Figure 10. Subsequently, Caspian Sea is simulated with real boundary conditions such as wind forcing, heat fluxes, precipitation via evaporation, river discharge with pollutant data and temperature. To verify the experimental results, there are compared with real conditions. In fact, for data and boundary conditions, CEPO (Caspian Environment Program Organization) and NOAA are used. The Caspian Sea Oceanographic and Environmental Data Inventory from CEPO are shown in Figure 11. In Figures 12 and 14, the results of simulations with data and boundary conditions from CEPO and NOAA are shown. Figures 13 and 15 show the real conditions in Caspian Sea. It is obvious from figures that

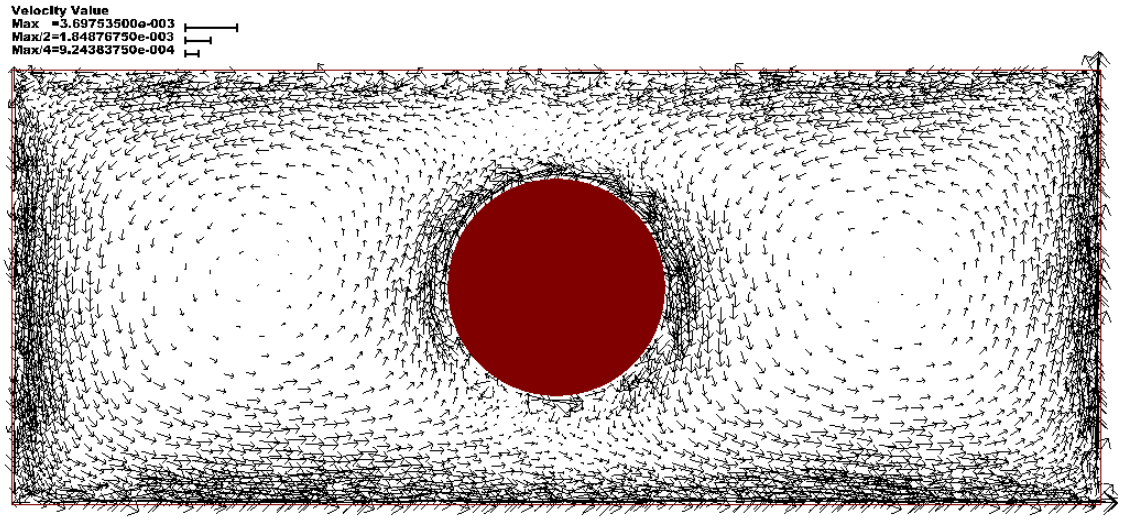

Figure 5. Velocity distribution for condition (I-1) with a circular island in the center of domain.

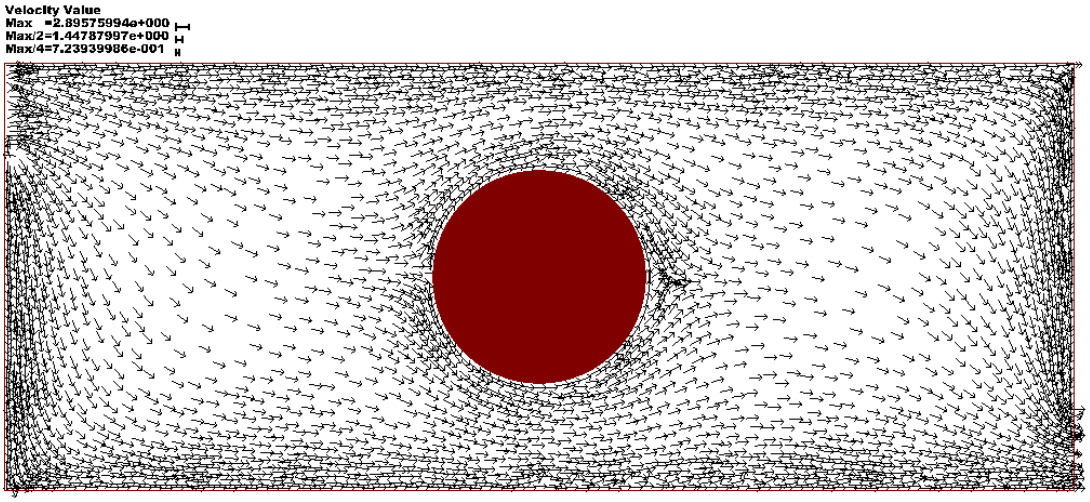

Figure 6. Velocity distribution for condition (I-4) with a circular island in the center of domain.

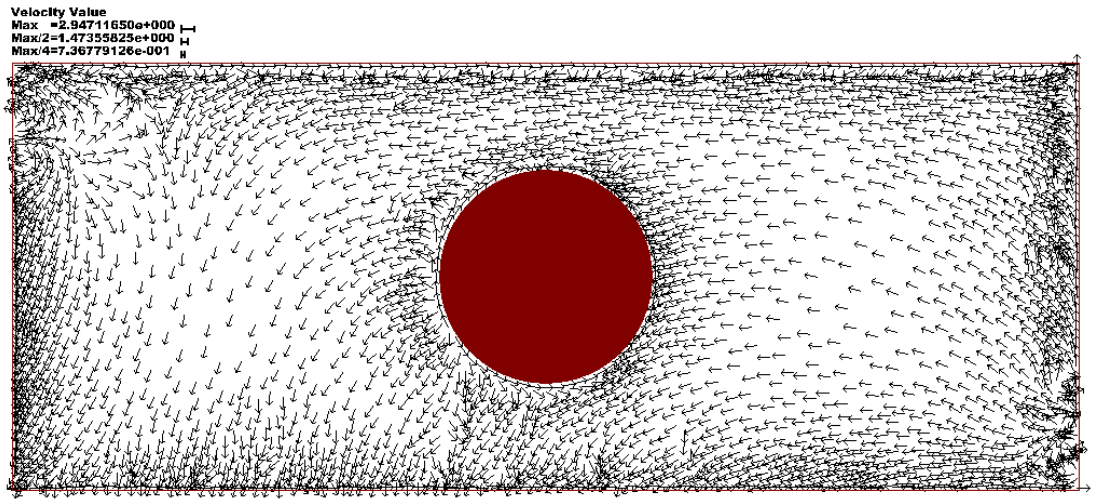

Figure 7. Velocity distribution for condition (I-5) with a circular island in the center of domain.

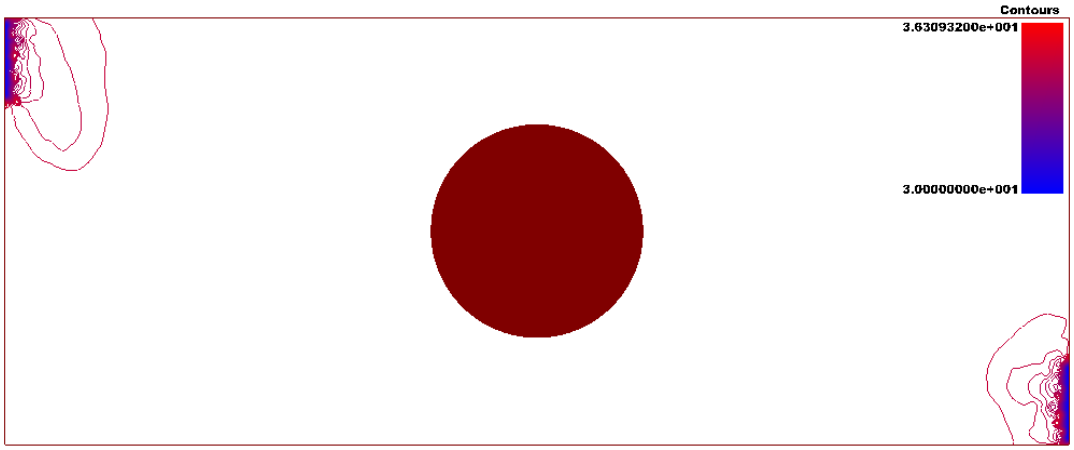

Figure 8. Salinity distribution for condition (II-4) with a circular island in the center of domain.

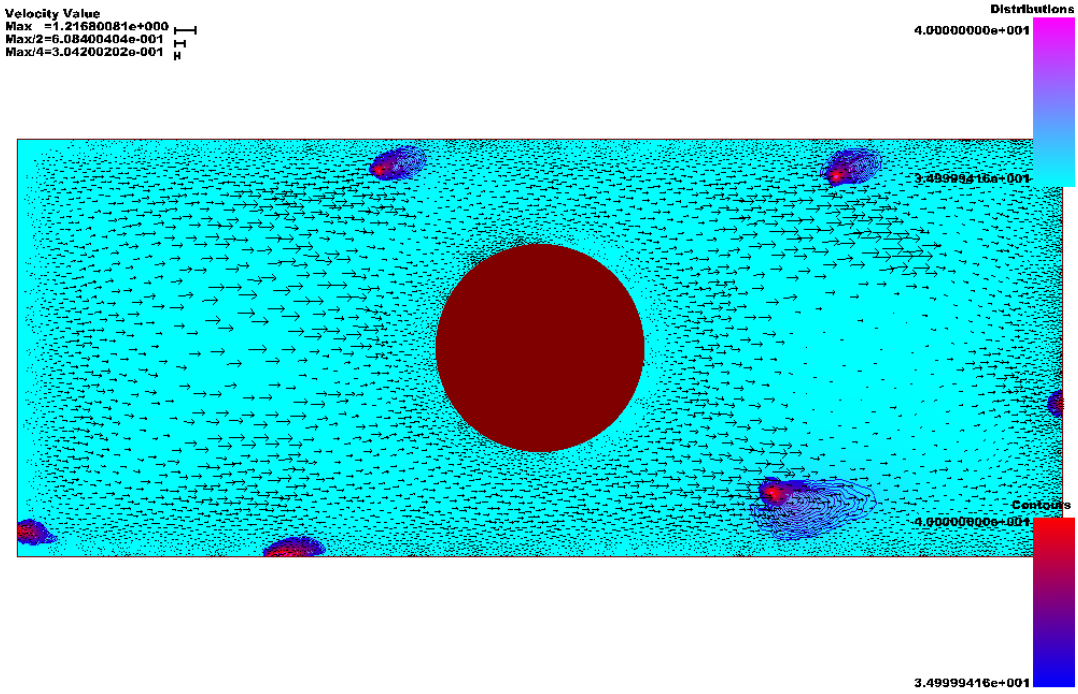

Figure 9. Velocity and pollutant distribution for condition (II-5) with a circular island in the center of domain.

the obtained simulation results are so close to the real conditions.

11. Conclusions

After numerous trials, it was discovered that those tidal elevations, precipitation and evaporation have little effect on pollutant distribution in Southern Caspian Sea. However, sea depth, the rate of discharge from incoming rivers, Coriolis force, wind force, cyclonic eddy currents and temperature changes were found to have a huge impact on the pollutant dispersion, especially in regions close to shore which have slow currents. The aggregated metal pollutant mostly consist of Aluminum case terrigenous material and the amount of fine-grained material present. An exception to this is Barium (Ba), for which the abnormal high concentrations are probably from drilling mud. Several metals such as Arsenic (As), chromium (Cr), and Nickel (Ni) exhibit concentrations sufficiently high to exceed sediment quality guidelines. Such metals undoubtedly have a high natural background in this mineral-rich region. However, anthropogenic activities such as mining, may have further enhanced the metal burdens in the sediments of the Caspian Sea. This might explain apparent hotspots for Copper (Cu) and Zinc (Zn) in Azerbaijan and Iran. Uranium (U) levels are generally

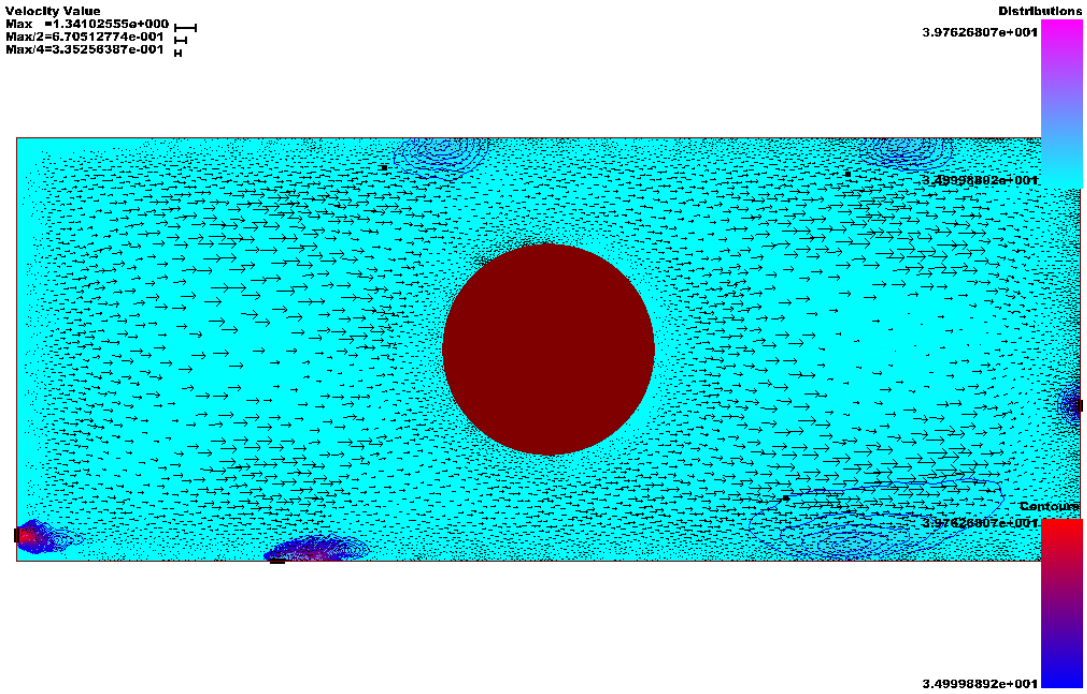

Figure 10. Velocity and pollutant distribution of domain after two weeks: one week with condition (II-5) and one week without any sources.

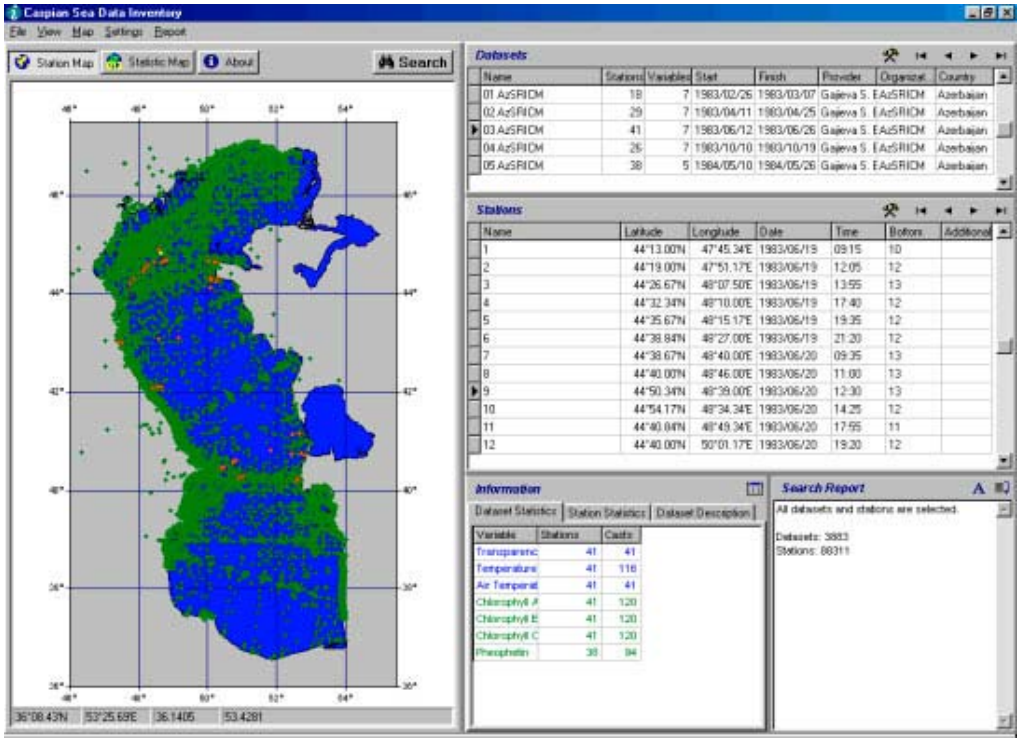

Figure 11. The Caspian Sea Oceanographic and Environmental Data Inventory.

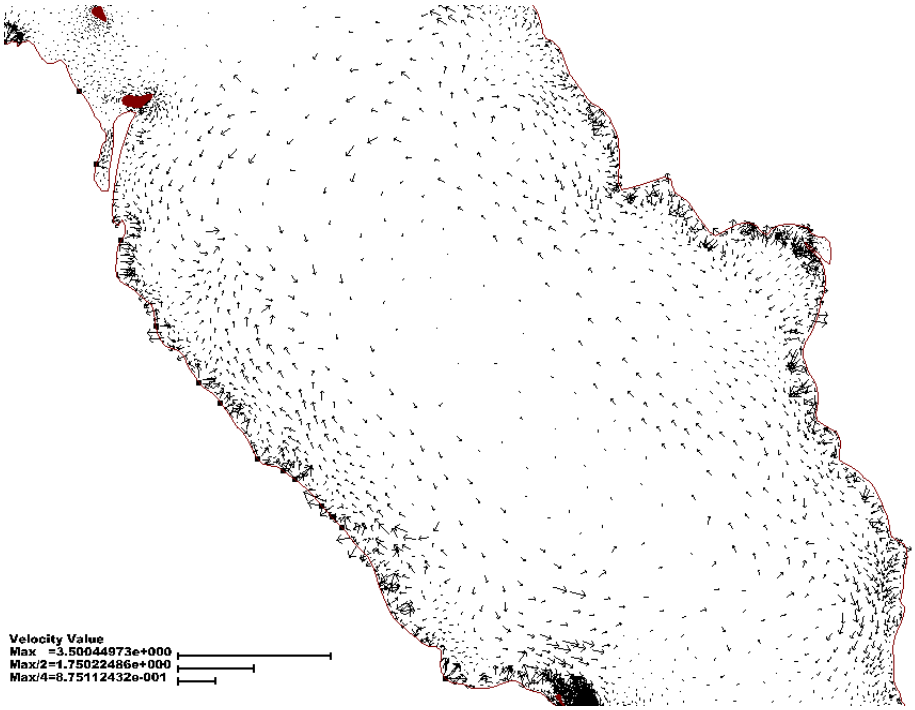

Figure 12. Circulation experimental run result for Caspian Sea after six months, zoom of middle region, σ=1 and only Coriolis force.

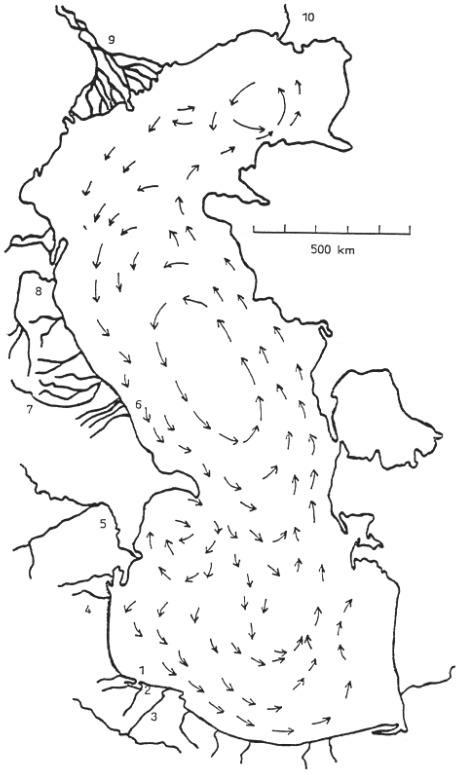

Figure 13. Schematic map showing the water circulation in the Caspian Sea (Apollov et al., 1969) 1: Bandar Anzali, 2: Anzali Lagoon, 3: Sefid River, 4: Astara River, 5: Kura River, 6: Keiranchai River, 7: Samur River, 8: Terek River, 9: Volga River, 10: Ural River.

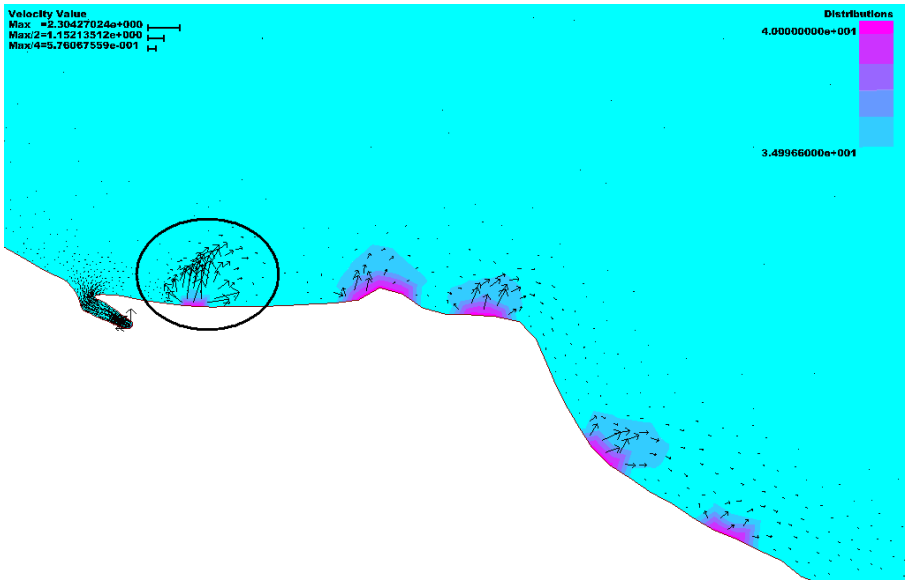

Figure 14. Experimental run result for pollutant and velocity distribution (in real boundary condition) of southwest of Caspian Sea after two weeks and σ=1.

Figure 15. Real velocity distribution of Bandar Anzali.

low (less than 3 μg·g^{-1}), except for a couple of sites in the central eastern Caspian Sea, where the concentration reaches 11.1 μg·g^{-1}. Some other metals such as Silver (Ag), Cadmium (Cd), and Lead (Pb) have relatively low levels that pose no environmental concerns.

References

Apollov, B.A., Evseeva, L.S., Kosarev, A.N. (1969). Dinamika vod, (Dynamics of water). In A.D.Dobrovol' skii, A.N.Kosarev, and O.K.Leont' eva (Eds.) Kaspiiskoe more. Izd. Moskovskogo Universiteta, Moskva. pp. 139-183. (In Russian)

Blumberg, A.F., Mellor, G.L. (1987). *A description of a three-dimensional coastal ocean circulation model*, Three-Dimensional Coastal Ocean Models, N. S. Heaps, Ed., Coastal and Estuarine Series, Amer. Geophys. Union, 4, 1-16.

Blumberg, A.F. (1994). *A Primer for Ecom-si. Tech. Rep.,* HydroQual, Inc., pp.66.

Chen, C., Zheng, L.Z., and Blanton, J.O. (1999). Physical processes controlling the formation, evolution, and perturbation of the low salinity front in the inner shelf off the southeastern United States: A modeling study, *J. Geophys. Res.*, 104, 1259-1288, doi:10.1029/1998JC900040.

Chen, J.Z., Ralph, E., Green, S.A., Budd, J.W., and Zhang, F.Y. (2001). Prognostic modeling studies of the Keweenaw Current in Lake Superior. Part I: Formation and evolution, *J. Phys. Oceanogr.*, 31, 379-395, doi:10.1175/1520-0485(2001)031.

Chen, C., Beardsley, R.C., Franks, P.J.S., and Keuren, J.V. (2003). Influences of the diurnally varying heat flux on stratification and residual circulation on Georges Bank, *J. Geophys. Res.*, 108 (C11), doi:10.1029/2001JC001245.

Cockburn, B., Hou, S., and Shu, C.W. (1990). TVB Runge-Kutta local projection discontinuous Galerkin finite element method for conservation laws, IV: The multidimensional case, *Math Comput.,* 54, 545-581, doi:10.1016/0021-9991(89)90183-6.

Dick, E. (1994). *Introduction to finite-volume techniques in computational fluid dynamics. Computational Fluid Dynamics*, J. F. Wendt, Ed., Springer-Verlag, pp. 271-297.

Haidvogel, D., Wilkin, J., and Young, R. (1991). A Semi-spectral Primitive Equation Ocean Circulation Model Using Vertical Sigma and Orthogonal Curvilinear Horizontal Coordinates, *J. Comput. Phys.,* 94, 151-184, doi:10.1016/0021-9991(91)90141-7.

Lynch, D.R., and Naimie, C.E. (1993). The M2 Tide and its Residual on the Outer Banks of the Gulf of Maine, *J. Phys. Oceanogr.*, 23, 2222-2253, doi:10.1175/1520-0485(1993)023<2222:TMTAIR>2.0.CO;2.

Maday, Y., and Patera, A.T. (1989). *Spectral element methods for the incompressible Navier-Stokes equations*, State-of-the-Art Surveys on Computational Mechanics, A. K. Noor, Ed., ASME, 71-143.

Marshall, J., Adcroft, A., Hill, C., Perelman, L., and Heisey, C. (1997). A finite-volume, incompressible Navier-Stokes model for Studies of the Ocean on Parallel Computers, *J. Geophys. Res.*, 102, 5753-5766.

Marshall, J., Hill, C., Perelman, L., and Adcroft, A. (1997). Hydrostatic, Quasihydrostatic and Non-hydrostatic Ocean Modeling, *J. Geophys. Res.*, 102, 5733-5752.

Mellor, G.L., and Yamada, T. (1982). Development of a Turbulence Closure Model for Geophysical Fluid Problems, *Rev. Geophys. and Space Phys.,* 20(4), 851-875.

Mellor, G.L., Hakkinen, S., Ezer, T., and Patchen, R. (2002). *A Generalization of a Sigma Coordinate Ocean Model and an Intercomparison of Model Vertical Grids, in Ocean Forecasting: Conceptual Basis and Applications*, N. Pinardi and J. D. Woods (Eds.), Springer, Berlin, 55-72.

Mellor, G.L. (1998). Users Guide for a Three-dimensional Primitive Equation, Numerical Ocean Model, *Program in Atmospheric and Oceanic Sciences*, Princeton University, Princeton, NJ 08544-0710.

Naimie, C.E. (1996). Georges Bank residual circulation during weak and strong stratification periods: Prognostic numerical model results, *J. Geophys. Res.,* 101, (C3), 6469-6486.

Reed, W.H., and Hill, T.R. (1973). *Triangular and methods for the neutron transport equation*, Tech. Rep. LA-UR-73-479, Los Alamos Scientific Laboratory.

Sverdrup, H., Johnson, M., and Fleming, R. (1942). *The Oceans: Their Physics, Chemistry and Biology*, Prentice Hall, New York, 1060

Ward, M.C. (2000). An Unsteady Finite Volume Circulation Model, Estuarine and Coastal Modeling, *Proceedings of the 6th International Conference*, November 3-5, 1999, New Orleans, Louisiana, M. L. Spaulding and H. L. Butler, Eds., ASCE, pp. 17-33.